X CONGRESSO NACIONAL DE ENGENHARIA MECÂNICA 2018
20 A 24 DE MAIO DE 2018 SALVADOR – BA – BRASIL

Finite Element Analysis applied to the Cooling of Electronic Components

L. H. CARNEVALE, lh.carnevale@gmail.com
G. R. ANJOS, gustavo.anjos@uerj.br
N. MANGIAVACCHI, norberto@uerj.br

Group of Environmental Studies for Water Reservoirs - GESAR, State University or Rio de Janeiro - UERJ, Rua Fonseca Teles, 121, 20940- 903, São Cristóvão, Rio de Janeiro, RJ, Brazil

Abstract: *The numerical simulation is an important tool to solve problems found in several physical processes, such as oil drilling, reservoir filling, hemodynamics and cooling of electronic components, the latter of great importance for describing problems related to controling flow and temperature conditions for new generation of stack processors. It is in this scope this project retains, for the development and improvement of a numerical platform using finite elements method simulation in order to study, in details, physical processes involved in cooling the eletronic components, specifically the characterization of temperature distribution in flows within different geometry. With this project, the objective is to comprehend, in detail, the mechanisms of heat dissipation in modern electronic components. Furthermore, it is also desired to have a better understanding of which alternatives present the most efficient cooling.*
Keywords: *Finite Element Method, Complex Geometries, Cooling of Electronic Components*

1. INTRODUCTION

Nowadays, most of the cooling devices found in personal computers or datacenters work with air or an hydraulic system. With the large increase in processing power and, therefore, performance enhencement of microprocessors, the temperature control of a computer chip became an extremely important and necessery task to ensure a precise and efficient operation, and moreover it improves the working life of those electronic components. Furthermore, the growing number of processors in each motherboard implicates in the assembly of multi-layer stacks of those components with internal refrigeration channels, as higher computational resources are required.

It is known that heat transfer is highly dependent on the nature of the flow contained in the observed system, and in this sense, Marcinichen and Thome (2010) and many other researchers have studied the multi-microchannel two-phase refrigerant evaporation for the simultaneous cooling of two or more stacked microprocessors. The usage of greenhouse refrigerant fluids that don't bring harm to the environment is an advantage to the method. The two-phase flow approach comes with greater difficulty in designing and modeling the cooling systems. On the other hand, as the flow uses the latent energy of the fluid substance to remove heat, it is observed a greater increase in the heat transfer coefficient that make the usage of microchannel evaporators a viable choice.

The Finite Element Method (FEM) formulation proposed uses the Galerkin method to discretize the spatial terms of the differential equation that model the heat transfer, together with a forward finite difference approximation to discretize the time derivatives (Lewis *et al.*, 2004). The resulting system of equations was solved using a direct method.

In this paper we numericaly implement a similar experiment as the one made by Szczukiewicz (2012) using different cross section geometries in the ducts that stay between the layers of processors, and as a first approach, calculating only the temperature distribution in the evaporator solid region and using a convection heat flux condition on the ducts boundary. In spite of cutting edge experimental techniques available, the numerical analysis has become an useful tool to simulate the behavior of the fluid flow and the heat transffer that occur in the proposed system due to the fast growth of computacional resources and its significant price reduction in comparison with experimental facilities.

2. MATHEMATICAL MODEL

2.1 Equations

A two dimensional Finite Element Method approach can be employed to analyse different physical phenomena that appear in engineering problems. The analysis of a problem starts with the mathematical modeling, and in this paper we use the Heat Transport Equation 1 over the domain Ω and with a variable thermal diffusivity $\alpha = k/\rho c_p$ (ρ is the density and c_p the specific heat) as a function of space. The boundary can be separeted in two regions $\Gamma = \Gamma_1 \cup \Gamma_2$, on Γ_1 it is applied a convection heat flux (q_{conv}) boundary condition and on Γ_2 the heat flux $\bar{q}$ is defined as the boundary condition.

$$\frac{\partial T}{\partial t} + \mathbf{v} \cdot \nabla T = \nabla \cdot (\alpha \nabla T) + Q \tag{1}$$

$$q_{conv} = h(T - T_\infty) \tag{2}$$

$$\left.\frac{\partial T}{\partial n}\right|_{\Gamma_1} = \frac{-q_{conv}}{k} = \frac{-h}{k}(T - T_\infty) \tag{3}$$

$$\left.\frac{\partial T}{\partial n}\right|_{\Gamma_2} = \frac{-\bar{q}}{k} \tag{4}$$

Where T is the scalar field of temperature, $\mathbf{v}$ is the velocity field, Q is the generation of heat, t is the time variable, h is the heat transfer coefficient, k is the thermal condutivity, and T_∞ is the temperature of the fluid promoting the convection heat flux. The terms $\frac{\partial T}{\partial n}$ indicate differentiation on the direction normal to the boundary.

In this paper we are interested in observing the temperature distribution over a solid region and no heat generation is considered ($\mathbf{v} = 0$ and $Q = 0$), thus Eq. 1 is reduced to:

$$\frac{\partial T}{\partial t} = \nabla \cdot (\alpha \nabla T) \tag{5}$$

For Eq.5 a non-dimensional form can be deduced as demonstrated in (HAHN and ÖZIŞIK, 2012, p. 25) using the non-dimensional variables:

$$T^* = \frac{T - T_\infty}{T_0 - T_\infty}\,, \quad t^* = \frac{\alpha t}{L^2}\,, \quad x^* = \frac{x}{L}\,, \quad y^* = \frac{y}{L}\,, \quad \alpha^* = \frac{\alpha}{\alpha_0}\,, \quad \rho^* = \frac{\rho}{\rho_0}\,, \quad c_p^* = \frac{c_p}{c_{p0}} \tag{6}$$

Dropping the non-dimensional notation, Eq. 5 keeps the same form, however, it is important to notice that α is kept in the equation as a value relative to a reference. The variables ρ_0 and c_{p0} are reference values and T_0 is a reference temperature. The convection heat flux condition (Eq. 3) becomes:

$$\alpha \left.\frac{\partial T}{\partial n}\right|_{\Gamma_1} = \frac{-Bi}{\rho c_v} T \tag{7}$$

where $Bi = \frac{hL}{k}$ is the Biot number (L is a characteristic length) and $c_v = c_p$ for solid materials.

2.2 FEM Formulation

Using the semi-discrete Galerkin method Eq. 5 is multiplied by a weight function w and integrated over the domain Ω.

$$\int_\Omega w \frac{\partial T}{\partial t} d\Omega - \int_\Omega w \, \nabla \cdot (\alpha \nabla T) d\Omega = 0 \tag{8}$$

Using the Green theorem on the diffusive term, Eq. 8 becomes:

$$\int_\Omega w \frac{\partial T}{\partial t} d\Omega + \int_\Omega (\nabla w) \cdot (\alpha \nabla T) d\Omega - \int_\Gamma w \left[(\alpha \nabla T) \cdot \mathbf{n}\right] d\Gamma = 0 \tag{9}$$

The integral evaluated over Γ represents the boundary conditions of the problem and the term $(\alpha \nabla T) \cdot \mathbf{n}$, when divided by ρc_p, represents the heat flux $q = q_{conv} + \bar{q}$ that passes through the boundary. Being ne the number of elements on the domain, the weight function and temperature are approximated by:

$$\begin{aligned} w &\approx \sum_j^{ne} b_j(t) \mathbf{N}_j(x, y) \\ T &\approx \sum_i^{ne} a_i(t) \mathbf{N}_i(x, y) \end{aligned} \tag{10}$$

Writing Eq.9 with Eq. 10, and not writing the sum notation:

$$\int_\Omega b_j \mathbf{N}_j \frac{\partial a_i \mathbf{N}_i}{\partial t} d\Omega \; + \int_\Omega \nabla(b_j \mathbf{N}_j)\, \alpha \nabla(a_i \mathbf{N}_i)\, d\Omega \; = - \int_\Gamma b_j \mathbf{N}_j \; \frac{q}{\rho c_p} \; d\Gamma \tag{11}$$

The integral over Γ can be separeted in two regions, one with the convection heat flux (Γ_1) and other with a defined flux(Γ_2).

$$\int_\Gamma \mathbf{N}_j \; \frac{q}{\rho c_p} \; d\Gamma = \int_{\Gamma_1} \mathbf{N}_j \; \frac{Bi}{\rho c_p} a_i \mathbf{N}_i \; d\Gamma_1 + \int_{\Gamma_2} \mathbf{N}_j \; \frac{\bar{q}}{\rho c_p} \; d\Gamma_2 = Bi \; a_i \int_{\Gamma_1} \mathbf{N}_j \; \frac{1}{\rho c_p} \mathbf{N}_i \; d\Gamma_1 + \mathbf{f} \tag{12}$$

Definig the mass matrix $\mathbf{M}$ over the domain Ω, the stiffness matrix $\mathbf{K}$, and the mass matrix $\mathbf{m}$ over the boundary Γ_1 as:

$$\int_\Omega \mathbf{N}_j \mathbf{N}_i d\Omega = \mathbf{M} \tag{13}$$

$$\int_\Omega \nabla \mathbf{N}_j \; \alpha \nabla \mathbf{N}_i \; d\Omega = \mathbf{K} \tag{14}$$

$$\int_{\Gamma_1} \mathbf{N}_j \; \frac{1}{\rho c_p} \mathbf{N}_i \; d\Gamma_1 = \mathbf{m} \tag{15}$$

substituting Eqs.14, 13, 12, 15 in Eq. 11:

$$\mathbf{M} \frac{\partial a}{\partial t} + (\mathbf{K} + Bi \; \mathbf{m}) a = \mathbf{f} \tag{16}$$

A forward difference approximation with the semi-implicit method was used to approximate the time derivative in Eq. 16:

$$\left(\frac{\mathbf{M}}{\Delta t} + \theta(\mathbf{K} + Bi \; \mathbf{m}) \right) a^{n+1} = \left(\frac{\mathbf{M}}{\Delta t} - (1-\theta)(\mathbf{K} + Bi \; \mathbf{m}) \right) a^n + \mathbf{f} \tag{17}$$

The variable θ can have values between 0 and 1 for an explicit or implicit method respectively. When $\theta = 0.5$ it is known as the Crank-Nicolson method.

2.3 Geometry And Mesh

The different cross section geometries used in this paper were dimensioned to have the same hydraulic diameter D_h and all of the solid domain is a $5D_h \times 7D_h$ rectangle divided in two regions, above and below $3D_h$, that correspond to different materials. The goal of these simulations is to represent the experimental set-up used by Szczukiewicz (2012).

For the mesh generation we use a Delaunay triangulation option present on the open source software "GMSH" Geuzaine and Remacle (2009). This choice was made to facilitate the implementation of a FEM algorithm because linear triangular meshes have well known shape functions (e.g. Lewis *et al.*, 2004, p. 49) and the integrals in the formulation can be easily calculated. All the unstuctured meshes with complex geometries used in this paper are presented in Fig. 1.

The hydraulic diameter is calculated by:

$$D_h = \frac{4A}{P} \tag{18}$$

where A is the area of the duct cross section, and P the perimeter. For the elliptical section, the parameters a and b were obtaind by choosing a value for a and using Eq. 19 as the perimeter approximation.

$$P \approx \pi(a+b) \left(1 + \frac{3h}{10 + \sqrt{4 - 3h}} \right) \texttt{and}, \;\; h = \frac{(a-b)^2}{(a+b)^2} \tag{19}$$

Setting $D_h = 1$, the parameters and dimensions of the geometries and meshes are presented in Tab. 1.

Duct Cross Section	Dimensions	Number of Nodes	Number of Elements
Square	$l = 1$	1308	2616
Equilateral Triangle	$l = 1.73205$	1250	2500
Circle	$d = 1$	1646	3292
Ellipse	$a = 1.436\ b = 0.35$	1444	2888

Table 1: Mesh parameters

The meshes used had their elements size set to be smaller in the interface between both material regions and also on the channel boundary with the intent to obtain better results, and to reduce the computational power needed to solve the systems of equations by reducing the number of elements on the rest of the domain.

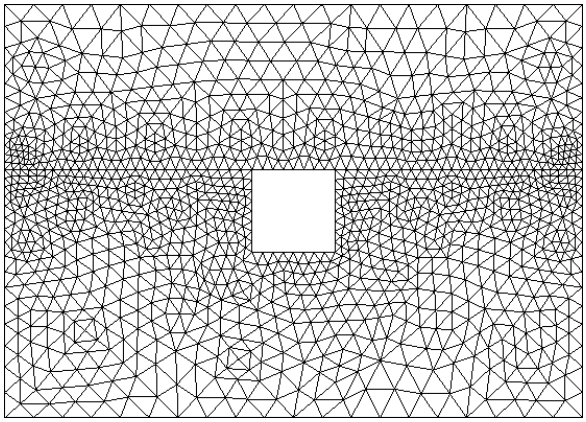

(a) Square with nodes and elements

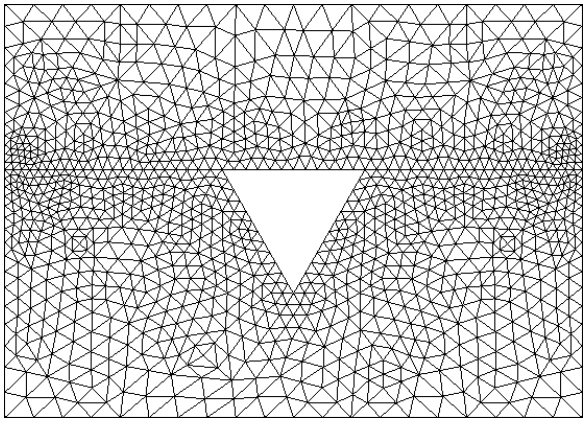

(b) Equilateral triangle with nodes and elements

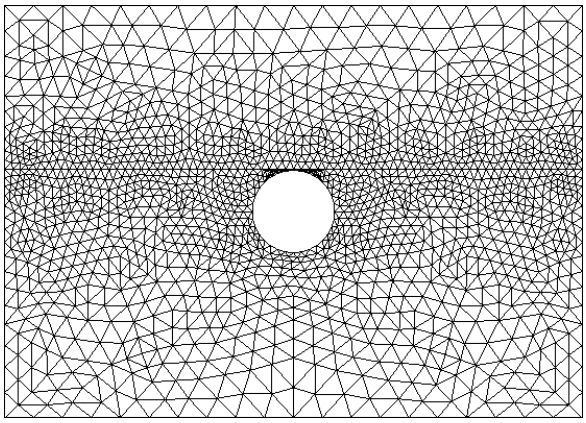

(c) Circle with nodes and elements

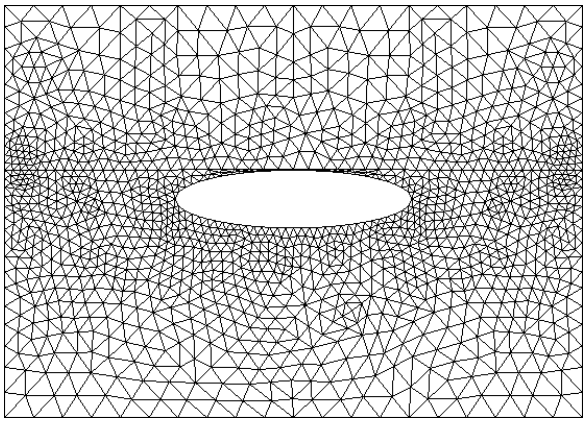

(d) Elipse with nodes and elements

Figure 1: Linear triangular meshes with different channel geometries generated with the software "GMSH"

3. RESULTS

3.1 Validation

As a validation test, the following problem with the Laplace equation and Dirichlet boundary conditions is proposed:

$$\begin{cases} \nabla^2 u(x,y) = 0 \\ u(0,y) = 0 \\ u(x,0) = 0 \\ u(x,2) = 0 \\ u(3,y) = f(y) \end{cases} \qquad \texttt{and,} \qquad f(y) = \begin{cases} y, & 0 \leq y \leq 1 \\ 2 - y, & ,1 \leq y \leq 2 \end{cases} \tag{20}$$

The problem can be solved by separation of variables and its solution is given by Eq. 21. A comparison between the analytical and numerical solution obtained by the FEM algorithm is demonstrated in Fig. 2.

$$u(x,y) = \frac{8}{\pi^2} \sum_{m=1}^{\infty} \frac{\sin\left(\frac{m\pi}{2}\right)}{m^2 \sinh\left(\frac{3m\pi}{2}\right)} \sinh\left(\frac{m\pi x}{2}\right) \sin\left(\frac{m\pi y}{2}\right) \tag{21}$$

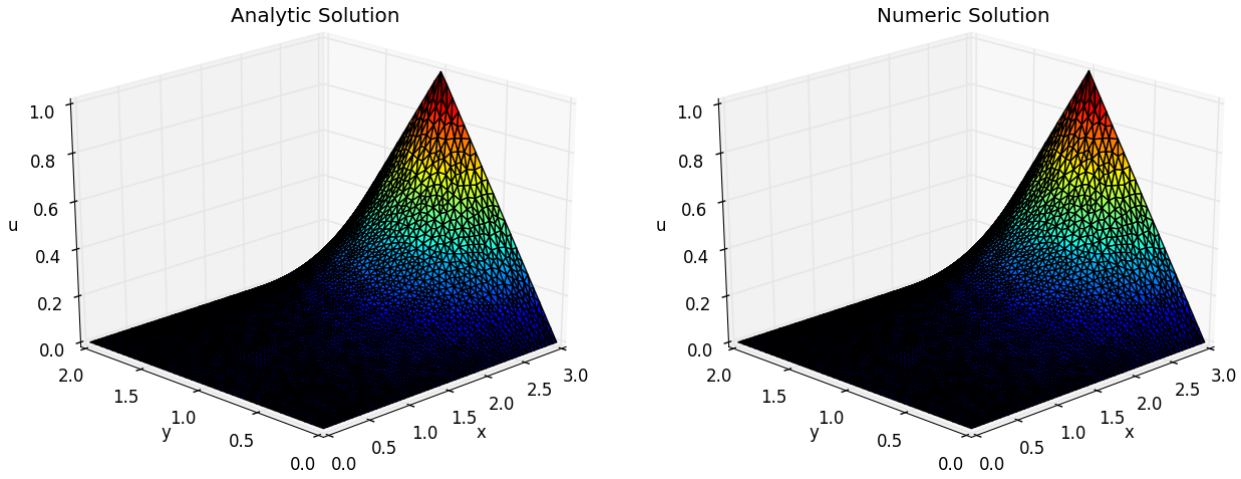

Figure 2: Comparison between analytical and numerical solution on a mesh with 3288 nodes and 6576 elements

A convergence analysis using the L^2 norm and six meshes with 24, 106, 402, 828, 1343, 3288 nodes is shown in Fig. 3. From this graphic, it is possible to notice the numerical method achieves a quadratic convergence rate. Being $\bar{u}_i$ the analytic solution and u_i the numeric solution at node i, the error is:

$$Error = \sqrt{\sum_{i}^{nodes} (\bar{u}_i - u_i)^2} \tag{22}$$

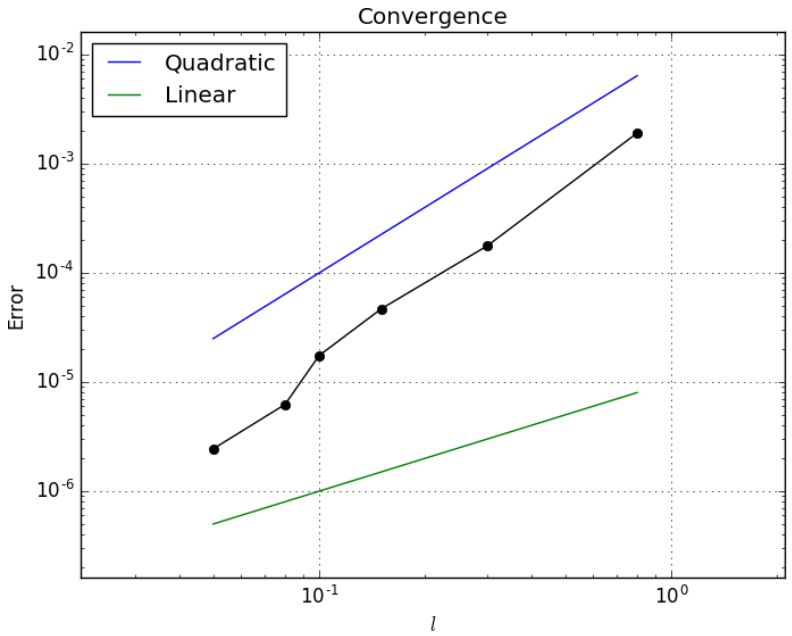

Figure 3: Convergence of the algorithm using L^2 norm, the characteristic length of the elements (l) were set in "GMSH" as 0.8, 0.3, 0.15, 0.1, 0.08, 0.05

3.2 Micro Evaporator Channel Geometries

The open source software “PARAVIEW” Ahrens *et al.* (2005) was employed for post-processing and analysis of the numerical solutions obtained, making it possible to visualize the data through different tools such as geometric sections, interpolations and vectorization.

All the geometries were simulated using the same parameters and boundary conditions. For the different materials, we used the same as in Szczukiewicz (2012), and their properties are described in Tab. 2.

Material	Region (μm)	k ($\frac{W}{m.K}$)	ρ ($\frac{kg}{m^3}$)	c_p ($\frac{J}{kg.K}$)
Silicon	$0 \leq y < 300$	159	2329	712
Pyrex	$300 \leq y \leq 500$	1.2	2230	800

Table 2: Materials properties

Using the silicon as the reference material ($\rho = k = c_p = 1$), the pyrex relative properties are $k = 0.007547$, $\rho = 0.957492$ $c_p = 1.123595$. The spatial measures were non-dimensionalized with $L = 100\mu m$ The boundary conditions represented in Fig. 4 were the same for the other channel geometries.

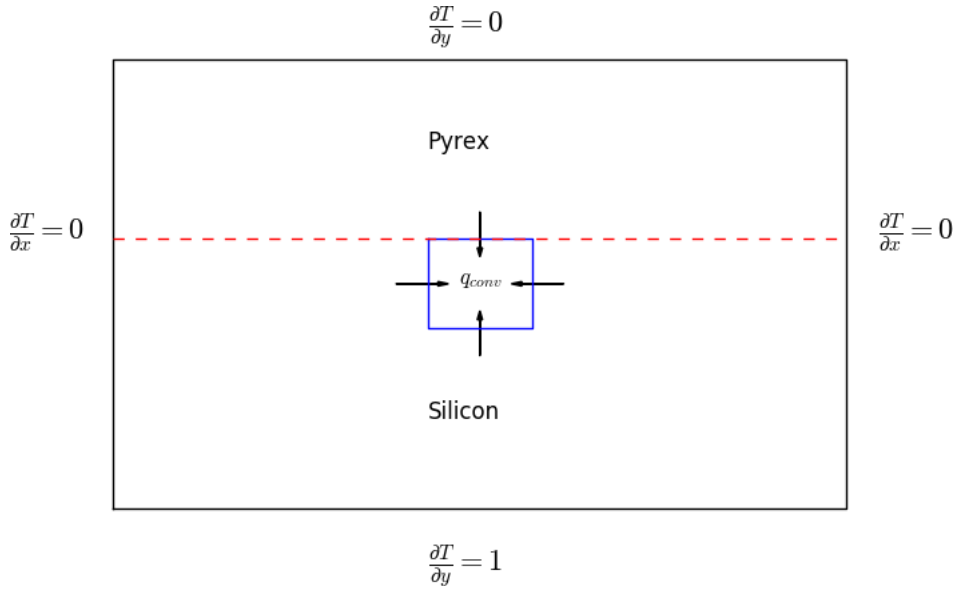

Figure 4: Boundary conditions, material regions, and geometry in the square channel case. The solid region has a length = 7 and height = 5, the pyrex region is above height = 3

The simulation was set to have a total of 600 iterations over time with $\Delta t = 0.01$ and the Crank-Nicolson method was used ($\theta = 0.5$). For each geometry two cases were tested, one with $Bi = 1$ and the other with $Bi = 100$.

In Fig. 5 the time development of temperature on the silicon and pyrex structure with flow in a square channel cross section is presented for both values of the Biot number.

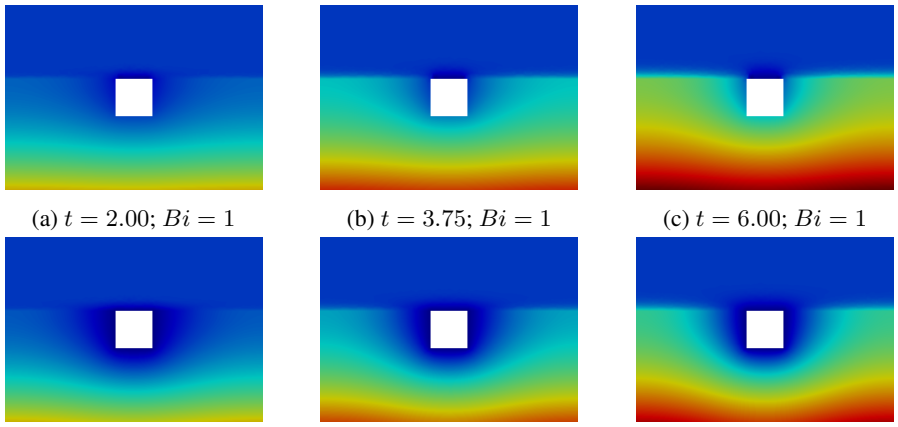

(a) $t = 2.00$; $Bi = 1$ (b) $t = 3.75$; $Bi = 1$ (c) $t = 6.00$; $Bi = 1$

(d) $t = 2.00$; $Bi = 100$ (e) $t = 3.75$; $Bi = 100$ (f) $t = 6.00$; $Bi = 100$

Figure 5: Temperature distribution on the silicon and pyrex region with a square cross section channel

In Fig. 6 the time development of temperature on the silicon and pyrex structure with a triangular duct cross section is presented using the same iterations as the square channel result and it also shows both Biot number cases.

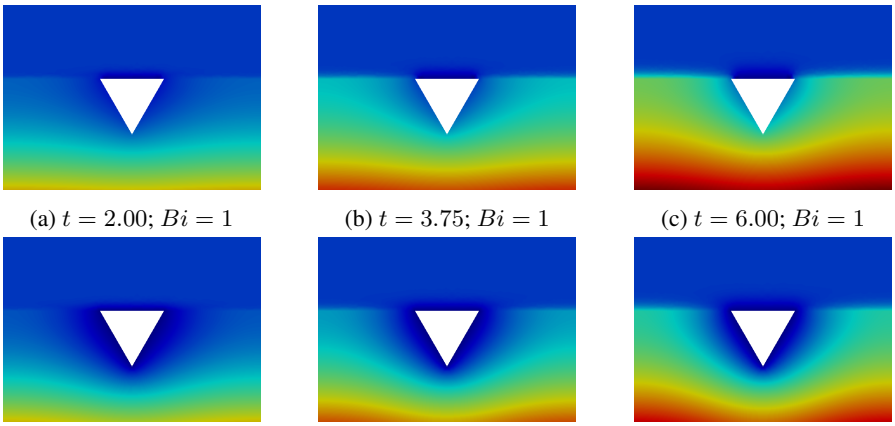

(a) $t = 2.00$; $Bi = 1$ (b) $t = 3.75$; $Bi = 1$ (c) $t = 6.00$; $Bi = 1$

(d) $t = 2.00$; $Bi = 100$ (e) $t = 3.75$; $Bi = 100$ (f) $t = 6.00$; $Bi = 100$

Figure 6: Temperature distribution on the silicon and pyrex region with a triangular cross section duct

The time development of temperature on the silicon and pyrex structure with a circular channel cross section is shown in Fig. 7 in the same manner as the previous results.

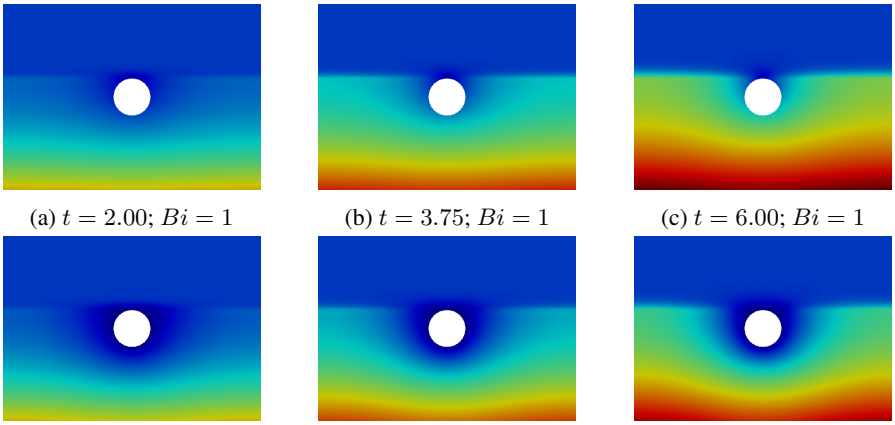

(a) $t = 2.00$; $Bi = 1$ (b) $t = 3.75$; $Bi = 1$ (c) $t = 6.00$; $Bi = 1$

(d) $t = 2.00$; $Bi = 100$ (e) $t = 3.75$; $Bi = 100$ (f) $t = 6.00$; $Bi = 100$

Figure 7: Temperature distribution on the silicon and pyrex region with a circlar cross section channel

The results obtainded for an elliptical channel cross section are demonstrated in Fig. 8 using the same iterations and Biot number. All the results had the same colormap scale. It is important to mention that in the pyrex region there was very little heat conduction due to a low relative thermal condutivity of the material and this fact made it difficult to set a colormap scale to showcase the phenomena in both regions, therefore only the silicon temperature distribution is observed as it is the material used in electronic components manufacturing.

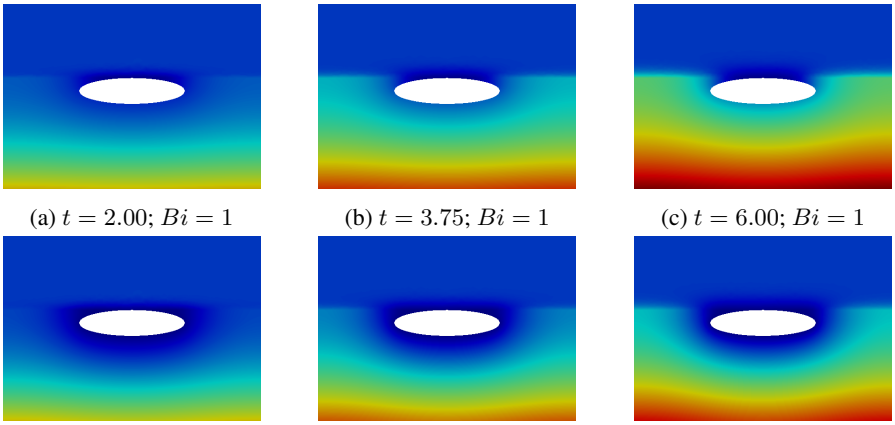

(a) $t = 2.00$; $Bi = 1$ (b) $t = 3.75$; $Bi = 1$ (c) $t = 6.00$; $Bi = 1$

(d) $t = 2.00$; $Bi = 100$ (e) $t = 3.75$; $Bi = 100$ (f) $t = 6.00$; $Bi = 100$

Figure 8: Temperature distribution on the silicon and pyrex region with an elliptical cross section channel

4. CONCLUSION

In this paper, a finite element method was developed to simulate the temperature distribution in complex cross section geometries of a possible heat exchanger used for cooling of electronic components. This method discretizes the governing

equations with the finite element method on unstructured triangular meshes. The results presented show a better heat transfer rate in the cases of higher Biot number, as expected, and the elliptical cross section has a better efficiency in cooling as the temperature distribution over the domain shows a smaller area with the highest temperature on the colormap scale when comparing with the other geometries.

5. ACKNOWLEDGEMENTS

The authors thank the FAPERJ (Research Support Foundation of the State of Rio de Janeiro) and CNPQ for their financial support.

6. REFERENCES

Ahrens, James, Geveci, Berk, Law and Charles, 2005. "Paraview: An end-user tool for large data visualization". URL `www.paraview.org`.

Geuzaine, C. and Remacle, J.F., 2009. "Gmsh: a three-dimensional finite element mesh generator with built-in pre- and post-processing facilities". *International Journal for Numerical Methods in Engineering*.

HAHN, D.W. and ÖZIŞIK, M.N., 2012. *HEAT CONDUCTION*. John Wiley & Sons Ltd, 3rd edition.

Lewis, R.W., Nithiarasu, P. and Seetharamu, K.N., 2004. *Fundamentals of the Finite Element Method for Heat and Fluid Flow*. John Wiley & Sons Ltd.

Marcinichen, J.B. and Thome, J.R., 2010. "Refrigerated cooling of microprocessors with micro-evaporation a new novel two-phase cooling cycles: A green steady-state simulation code". *Brazilian Congress of Thermal Sciences and Engineering*.

Szczukiewicz, S., 2012. *Thermal and Visual Operational Characteristics of Multi-Microchannel Evaporators using Refrigerants*. Ph.D. thesis, ÉCOLE POLYTECHNIQUE FÉDÉRALE DE LAUSANNE.

7. RESPONSIBILITY NOTICE

The authors are the only responsible for the printed material included in this paper.